Thermal stability and thermoelectric properties of *p*-type $Ba_8Ga_{16}Ge_{30}$ clathrates

D. Cederkrantz,[1,a] A. Saramat,[2] G. J. Snyder,[2] and A. E. C. Palmqvist[1]
[1]*Department of Chemical and Biological Engineering, Chalmers University of Technology, SE-41296 Göteborg, Sweden*
[2]*Materials Science, California Institute of Technology, Pasadena, California 91125, USA*

(Received 1 July 2009; accepted 26 August 2009; published online 9 October 2009)

The thermal stability of *p*-type $Ba_8Ga_{16}Ge_{30}$ clathrates grown from gallium flux has been tested by heat treatment in low pressure Ar atmosphere at 400, 600, and 800 °C. Significant gallium loss was observed for all samples during heat treatment. The treatment at 400 °C does not significantly change the sample properties, and the samples remain *p*-type and comparable to the untreated, as-prepared, sample. At 600 °C the sample switches from extrinsic *p*-type to extrinsic *n*-type, presumably due to significant loss of Ga, and shows a high thermopower but a reduced electrical conductivity compared to as-made *n*-type samples. Surprisingly, after a thermal treatment at 800 °C, the crystal structure seemingly loses less Ga, only reducing the hole concentration to near intrinsic levels and thus has a negative impact on *ZT*. Regardless of the heat treatment temperature of the *p*-type samples the thermal conductivity remained exceptionally low, for some samples 0.9 W/m K. Heat treatment can thus greatly affect the thermoelectric properties of *p*-type $Ba_8Ga_{16}Ge_{30}$, but the crystal structure remains intact. © *2009 American Institute of Physics*. [doi:10.1063/1.3236635]

I. INTRODUCTION

With looming environmental problems and the prospect of dwindling fossil fuel resources, the need for a more effective use of the available energy is an ever increasing challenge for science and technology today. In many energy conversion processes involving combustion of a fuel, a large fraction of the energy content is lost as waste heat. If this waste heat could be utilized, the conversion rate and fuel economy of the processes would be greatly increased. One way to recover waste heat is to use thermoelectric (TE) materials to convert a temperature gradient to an electric potential that can drive an electric current. The use of TE materials today is limited due to the poor conversion rate, but new materials with improved efficiency are expected to favor the application of TE generators. To achieve higher conversion rate a material that combines good electrical conductivity (σ) and poor thermal conductivity (κ), with a high thermopower (or Seebeck coefficient *S*), is the goal, which is often expressed by the TE dimensionless figure of merit, $ZT = TS^2\sigma/\kappa$. Combining these properties may seem simple, but according to electrodynamics *S*, σ, and κ are all derived from the same electronic energy function and hence interconnected. Intricate crystal dynamics and material processing are therefore needed to decouple the parameters from each other. A foundation for finding new TE materials was formulated in the "phonon-glass electron-crystal" (PGEC) concept by Slack,[1] concluding that a good TE material should conduct heat like a glass and electricity like a crystal.

Semiconducting clathrates are a group of materials that has shown great promise to follow the PGEC concept, and they have been studied in the context of thermoelectrics since the second half of the 1990s.[2–26] A large number of clathrate compounds have now been studied, and most of them are *n*-doped type-I structures, with the most prominent of the type-I clathrates being $Ba_8Ga_{16}Ge_{30}$ with a *ZT* of 1.35 at 900 K.[27] All TE devices need both *n*- and *p*-type materials, which should be compatible with each other in terms of, e.g., thermal expansion, and it is therefore beneficial to find *p*-type clathrates of equal potential and stability. The amount of work published on *n*-doped clathrates greatly outweighs the work on *p*-doped clathrates, and the reason for this is that the structure disfavors bonds between trivalent (Ga) atoms.[28] In the case of, e.g., $Ba_8Ga_{16}Ge_{30}$, this favors a lower Ga/Ge ratio than the stoichiometric 16/30 ratio thus resulting in *n*-doped materials. Despite the difficulty in preparing *p*-type clathrates, $Ba_8Ga_{16}Ge_{30}$,[29–32] $Ba_8Ga_{16}Zn_xGe_{30-x}$,[33] $Ba_8Au_xGe_{46-x}$,[34] and $Ba_8Ni_{6-x}Ge_{30+x}$ (Ref. 35) have all been made *p*-doped. Very high *ZT* values were reported for *p*-$Ba_8Ga_{16}Ge_{30}$, but when high temperature measurements were conducted, loss of gallium from the samples was observed.[36] The stability of *p*-type $Ba_8Ga_{16}Ge_{30}$ and its usefulness in an application can thus be questioned. In this study the thermal stability of *p*-doped $Ba_8Ga_{16}Ge_{30}$ has been investigated in more detail, and the effects of different heat treatments on its TE properties and its stability for device application assessed.

II. EXPERIMENTAL METHODS

A. Synthesis

The synthesis of clathrate samples was done by direct reactions of high-purity elements, Ba (Sigma-Aldrich, 99.99%), Ga (Sigma-Aldrich, 99.9995%), and Ge (Sigma-Aldrich, 99.9999%). Stoichiometric amounts was used for *n*-doped $Ba_8Ga_{16}Ge_{30}$, whereas for *p*-doped $Ba_8Ga_{16}Ge_{30}$ ex-

[a]Electronic mail: daniel.cederkrantz@chalmers.se.

TABLE I. Sample series and heat treatments used to establish the thermal stability of *p*-$Ba_8Ga_{16}Ge_{30}$.

Sample	Initial doping	Heat treatment	Final doping
BGG1	*p*	None	*p*
BGG2	*p*	36 h at 400 °C	*p*
BGG3	*p* [a]	3×36 h^2 at 600 °C+36 h at 800 °C	*n*
BGG4a	*p*	3×36 h^2 at 800 °C	*p*
BGG4b	*p* [a]	3×36 h^2 at 800 °C	*p*
BGG5	*n* [a]	None	*n*

[a]Sample has been stored as powder for an extended time following the heat treatment.

cess Ga (four times the stoichiometric amount) was used as flux. Mixing of the elements was performed in a glove box (high-purity Ar atmosphere). The *n*-doped $Ba_8Ga_{16}Ge_{30}$ sample was prepared in a quartz crucible, whereas an alumina crucible was used during synthesis of the *p*-doped $Ba_8Ga_{16}Ge_{30}$ samples. Following mixing of the elements, the reaction vessel was sealed in a quartz tube, under argon atmosphere. The tube was then evacuated to a pressure of approximately 0.1 mbar and placed in a furnace (Theremolyne 21100 tube furnace equipped with a Eurotherm controller) and heated to 1050 °C over 11 h, cooled to 970 °C over 1.5 h, followed by a slow approach over 4 h to the annealing temperature (963 °C). The annealing time was 24 h and followed by a slow cooling over 3 h to 955 °C, and subsequently a more rapid cooling to room temperature. After completed synthesis the formed crystals were removed from the crucible. The *p*-doped $Ba_8Ga_{16}Ge_{30}$ crystals were separated from the molten excess gallium with a pincer, and the remaining excess gallium was removed with a brush and hot water. The *n*-doped $Ba_8Ga_{16}Ge_{30}$ crystals were collected by gently crushing the quartz crucible and carefully removing the quartz pieces. Following synthesis the sign of the majority charge carriers was analyzed by heating one side of the crystals and a measure of the voltage across the sample.[37]

B. Heat treatment of *p*-doped $Ba_8Ga_{16}Ge_{30}$

Following their synthesis a series of *p*-doped $Ba_8Ga_{16}Ge_{30}$ samples from the same synthesis batch was heat treated one at the time in alumina crucibles placed in an evacuated quartz chamber (Ar trace atmosphere at 0.1 mbar). The first sample was treated at 400 °C for 36 h, the second at 600 °C for 36 h, this treatment was repeated three times, and the third at 800 °C for 36 h, which was also repeated three times. For heating and cooling a temperature ramp rate of 100 °C/h was used. During the treatments elemental gallium was found to leave the clathrate crystals, and deposit on their outer surfaces. The gallium was carefully removed with brush and hot water, followed by drying at 100 °C, and analysis of the sign of the majority charge carriers, as described above, was performed after each treatment. The sample treated at 600 °C was subsequently treated for an additional 36 h in 800 °C to establish if the apparent change from *p*- to *n*-type was reversible. As-prepared *n*- and *p*-doped samples were used as references. Table I displays the sample series studied and the labels that will be referred to throughout the paper.

C. Density measurements

The density of selected samples was measured with a pycnometer (AccuPyc 1330, Micromeritics) under helium atmosphere, using the gas displacement method. Measurements were performed on samples of single crystals as well as powders. The samples were carefully dried for 1 h in 100 °C before measurements.

D. Powder XRD

Powder x-ray diffraction (XRD) was performed on ground samples using a Bruker XRD D8 Advance and monochromatic Cu $K\alpha1$ radiation. Data were collected using either a 15 min scan with scanning angles 17°–60°, or a 6 h scan with angles 10°–120°, suitable for Rietveld refinement.

E. Sample preparation

To enable property measurements of the samples they were grinded (by mortar), hot pressed, and cut into suitable specimens for analysis. The polycrystalline samples were hot pressed in high-density graphite dies (POCO), which resulted in samples with >95% of the theoretical density. The hot pressing was performed on tablets with a diameter of 12 mm and a thickness of 5–7 mm using a weight of approximately 1.10 t at 827 °C for 60 min under argon atmosphere prior to annealing at 827 °C for 60 min under vacuum of 80 μbars. The hot-pressed samples were cut into wafers between 1 and 2 mm thick using a low speed diamond saw and polished with a 3M (600) fine abrasive paper. Hot pressing was performed at Jet Propulsion Laboratory (JPL) in Pasadena, CA.

F. Electrical and thermal property measurements

The Seebeck coefficient S, electrical conductivity σ, and thermal conductivity κ were all measured under vacuum less than 1 μbar. The van der Pauw technique was utilized to determine electrical conductivity. Data were collected with a current of 10 mA and using pressure contacts of molybdenum. The Seebeck coefficient was measured with W/Nb thermocouples and a differential light-pipe system similar to the one described elsewhere.[38] Both heating and cooling data were acquired showing the same features, but for clarity only heating curves will be presented due to small hysteresis in some samples. Thermal diffusivity and heat capacity were measured using a laser-flash method (Netzsch LFA 457) with a pyroceram 9606 standard. Hall Effect measurements were done to characterize the carrier concentration, i. Hall data were collected using the van der Pauw technique with magnetic fields of approximately 2 T. The TE measurements were performed at the California Institute of Technology in Pasadena, CA.

FIG. 1. (Color online) As-prepared $Ba_8Ga_{16}Ge_{30}$ crystals grown in excess gallium.

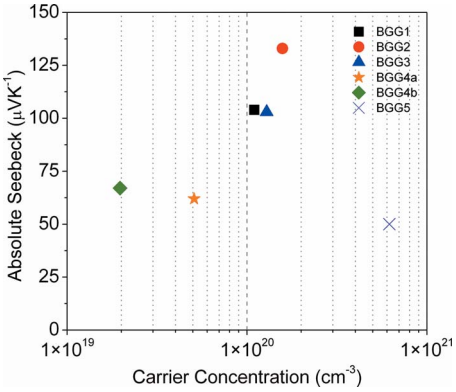

FIG. 2. (Color online) Absolute Seebeck coefficient vs charge carrier concentration at room temperature for $Ba_8Ga_{16}Ge_{30}$ samples described in Table I.

III. RESULTS AND DISCUSSION

A. Sample preparation and characterization

Powder x-ray diffractograms of all samples agreed well with the $Ba_8Ga_{16}Ge_{30}$ structure previously reported.[7] A characteristic Ge impurity phase[39] was found in the *n*-doped sample, while *p*-doped samples were all single phase or had very small amounts of impurity phase. Figure 1 shows as-prepared *p*-doped $Ba_8Ga_{16}Ge_{30}$ crystals of approximately 10 mm diameter and 3–4 mm thickness, and with clearly faceted and shiny surfaces. In Table II the weight decrease due to the loss of gallium during heat treatment is shown for all samples and found to be over 10 wt %. The room temperature density of the as-prepared and heat treated *p*-type samples was in the range 98.1%–98.6% of theoretical density, and thus did not change notably with heat treatment. This is explained by the small difference in density between Ga and the clathrate. After grinding, however, the powder density at room temperature was measured to be 100% of theoretical density, indicating enclosed voids in the crystals formed during synthesis.

B. TE evaluation

1. Charge carrier density and mobility

The absolute Seebeck coefficient is plotted versus the room temperature charge carrier concentration in Fig. 2. The *p*-type samples BGG1 and BGG2, and the *n*-type sample BGG3 all have a room temperature charge carrier concentration in the range $(1-2)\times10^{20}$ cm^{-3} while both BGG4a and BGG4b have lower carrier concentrations of 5×10^{19} and 2×10^{19}, respectively. The difference between the BGG4a and BGG4b samples may stem from their different physical shape during storage in ambient air, which for BGGa was a centimeter large piece and for BGG4b was powder. The smaller grain size will result in larger exposed specific surface area and shorter diffusion paths. In contrast the as-prepared *n*-doped sample, BGG5, exhibits the highest room temperature charge carrier concentration with 6×10^{20} cm^{-3}. The measured temperature-dependent charge carrier data (not shown) are scattered, but the trends are clear. The charge carrier concentration of BGG1 displays a linear increase up to $\sim4.5\times10^{20}$ cm^{-3} with increasing temperature, while the values for BGG2, BGG3, and BGG5 remain constant between room temperature and 400 °C. The BGG4a sample exhibits a slight increase in charge carrier concentration with temperature, while for BGG4b no trend could be discerned due to large scattering of the data above room temperature. The room temperature charge carrier density for samples BGG1–BGG4a agrees well with what is found in literature,[29,40] while the result for BGG4b is somewhat lower than previously reported for the $Ba_8Ga_{16}Ge_{30}$ system.

TABLE II. Weight loss due to heat treatment and sample densities after heat treatment, before and after grinding.

Sample	Weight loss after heat treatment (%)	Density after heat treatment[a]	Density after heat treatment and grinding[a]
BGG1	···	98.54	···
BGG2	10.9	98.30	···
BGG3	11.8	98.08	100
BGG4	22.6	98.64	100

[a]% of theoretical.

The charge carrier mobility of BGG1 and BGG2 is low (below 3 $cm^2/V\,s$) and remains more or less constant in the measured temperature range, from room temperature to 400 °C. Sample BGG4a shows similar low room temperature mobility, but at elevated temperatures electrons rather than holes seem to dominate the mobility, which is not unusual near an intrinsic transition. The data for BGG4b are very scattered and a trend cannot be extracted although a mean value yields very low mobility. Samples BGG3 and BGG5 have a higher mobility (11 and 7 $cm^2/V\,s$, respectively), which is consistent with previous reports on *n*-type $Ba_8Ga_{16}Ge_{30}$.[10,24]

2. Thermopower

In Fig. 3 the results from temperature-dependent *S* measurements from 30 to 700 °C are presented for all samples showing that samples BGG1, 2, 4a, and 4b are *p*-type while BGG3 and 5 are *n*-type. The measured *S* values of the untreated samples are comparable to previously published data for *p*-type[29] and *n*-type[27] $Ba_8Ga_{16}Ge_{30}$. Heating the *p*-type $Ba_8Ga_{16}Ge_{30}$ sample to 400 °C induces loss of gallium (perhaps only at grain boundaries) but not a transition to *n*-type.

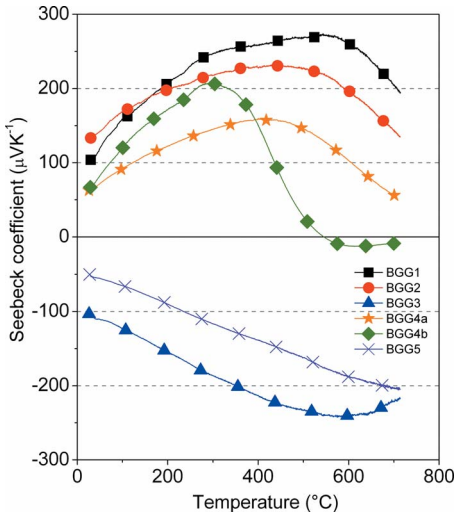

FIG. 3. (Color online) Thermopower as a function of temperature for $Ba_8Ga_{16}Ge_{30}$ samples described in Table I collected from room temperature to 700 °C.

The sample treated at 600 °C switched from being *p*-type before heat treatment to *n*-type after heat treatment, while the samples treated at 800 °C surprisingly remained *p*-type but with reduced hole concentration. To confirm this observation a number of *p*-type samples (not presented here) were prepared and heat treated in the same way after which the sign of the charge carriers was determined at room temperature as described earlier and were found to reproduce the same behavior. The additional treatment of the BGG3 sample at 800 °C did not reverse the charge carrier type, which shows that a 600 °C treatment results in irreversible conversion to *n*-type.

These trends in Seebeck correlate with differences in carrier concentration, which is presumably caused by the Ga content in the crystal structure. Most likely the Ga/Ge ratio is reduced by the Ga loss during annealing, which decreases the hole concentration. Reduction in the Ga/Ge ratio below 16/30 leads to the formation of *n*-type samples. It should be noted that the loss of Ga from the structure also must initially result in the formation of vacancies in the crystal structure. Ga and Ge occupy the crystallographic sites 6c, 16i, and 24k. Ga has a preference for the 6c site while Ge prefers the 16i site, and 24k is more equally preferred by the two elements.[28,41] The question as to whether the formed vacancies have any site preference remains to be determined, but the result of vacancies is half filled dangling bonds on the neighboring atoms. If the number of vacancies is high enough additional bands can be formed, which in turn can affect conduction and thermopower.[42–44] In the $Ba_8Ga_{16}Ge_{30}$ structure Ga acts as a single electron acceptor, while a Ga vacancy will act as a four electron acceptor, thus vacancies should cause the hole concentration to increase.[45,46] It therefore appears that the vacancies are filled with Ge and that the Ga leaves the structure, probably associated with a corresponding amount of Ba to balance the stoichiometry. At the annealing temperatures used the diffusion of Ge should be high enough to account for the filling of the vacancies, thus resulting in a structure with few vacancies and a low Ga/Ge ratio. A decrease in carrier concentration shifts the maximum of $|S|$ to lower temperatures due to the earlier onset of the intrinsic behavior, from 550 °C for BGG1 to 300 °C for BGG4b. Normally this also coincides with a larger maximum value of $|S|$ as seen when comparing the *n*-type BGG3 sample with the as-prepared BGG5 sample. The trend for *p*-type samples is unusual and may be due to variations within the sample, but when comparing the BGG4a and b the expected trend is clear.

It is not yet understood why there is a nonuniform trend on effect of heat treatment temperature on majority charge carrier type and why 600 °C produces more structural Ga loss than either 400 or 800 °C. The unexpected trend could be due to a competition between the kinetics and thermodynamics of Ga loss.

The effective mass was calculated from Eq. (1) using degenerate model with the charge carrier scattering distance independent of energy and room temperature data.[47]

$$S = \frac{8\pi^2 k_B^2}{3eh^2} m^* T \left(\frac{\pi}{3n}\right)^{2/3}, \tag{1}$$

where S is the thermopower, m^* is the effective mass, and n is the charge carrier concentration. The resulting average $m^* = 1.6 \pm 0.3 m_e$ was obtained from extrinsic samples (excluding BGG4a and b), where m_e is the free electron mass. Here the effective mass of holes is similar to that of electrons and comparable to previously reported data for electrons[10,24,25] while it is about half the previously reported values for holes.[10,30] The reason for the deviation between previously reported values of hole effective mass and the values reported here remains to be explained.

From the Seebeck data an approximation of the thermal band gap can be calculated according to[48]

$$E_g \sim 2S_{\max}T_{\max}. \tag{2}$$

A mean value of 0.4 ± 0.07 eV was obtained for E_g (again excluding near intrinsic samples BGG4a and b), which corresponds well with $E_g \sim 0.39$ eV reported by May *et al.*[49] In addition, the value reported here is consistent with theoretical estimate done by Blake *et al.*[6] (~0.5 eV), where calculations made by Madsen *et al.*[12] showed a somewhat larger E_g (~0.9 eV).

3. Electrical resistivity

Figure 4 shows the temperature-dependent electrical resistivity of the samples in Table I. The samples can be divided into three groups based on the magnitude of their resistivity. The *n*-doped samples BGG3 and BGG5 show a low resistivity at room temperature of less than 10 mΩ cm. The as-prepared and low temperature treated *p*-type samples BGG1 and BGG2 have a resistivity between 10 and 15 mΩ cm, whereas the high temperature treated samples BGG4a and BGG4b showed high resistivities of 34 and above 200 mΩ cm, respectively. The samples generally follow the trend expected from the carrier concentration measurements with higher carrier concentrations leading to lower resistivity.

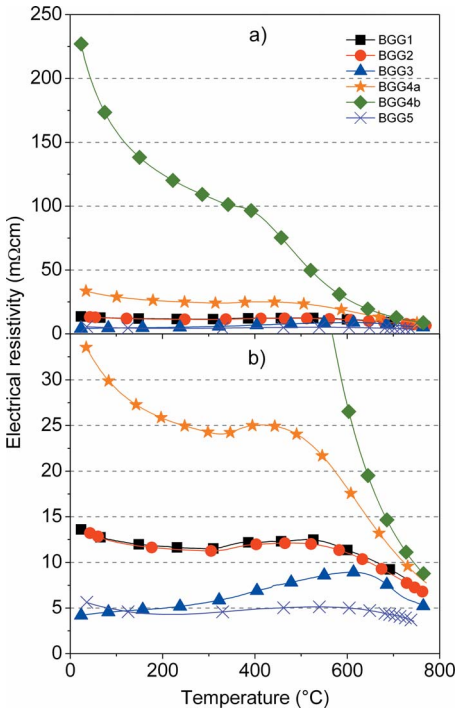

FIG. 4. (Color online) Electrical resistivity as a function of temperature for the $Ba_8Ga_{16}Ge_{30}$ samples presented in Table I. In (a) the full resistivity interval is shown while (b) shows the low resistivity region to highlight the trends of the data.

The resistivity for the *n*-type samples is somewhat higher than what has previously been reported. The linear increase with temperature until a maximum is reached around the intrinsic transition, which occurs at 600 °C for BGG3, is typical for heavily doped semiconductors.[24] This behavior is not as clear for BGG5. Samples BGG1 and BGG2 have almost identical resistivity, which further shows that the treatment at 400 °C only has a small impact on the TE properties restricted to a limited increase in charge carrier concentration. As seen in Fig. 4 the electrical resistivity of these *p*-type samples exhibits a maximum similar to that observed for the heavily doped *n*-type case, but does not exhibit the linear increase up to the maximum that was observed for BGG3. Instead a shallow minimum is found in the intermediate temperature range, which could be related to the lower charge carrier concentration for the *p*-doped samples similar to that seen in *n*-type samples.[49] Both samples BGG4a and BGG4b show elevated resistivity although with largely different values. The resistivity of BGG4a falls from 34 mΩ cm at room temperature to levels comparable with the other samples at 750 °C, while BGG4b shows a resistivity of over 225 mΩ cm at room temperature, which subsequently drops to the same level as the other *p*-type samples at 750 °C. A local maximum in resistivity can be found around 400 °C for both samples, but occurring at somewhat lower temperature for BGG4b. The difference in room temperature resistivity and the shifted maximum are reflected in the Seebeck measurements where BGG4b shows the onset of its intrinsic transition at a lower temperature than BGG4a, which in turn has its intrinsic transition onset at a lower temperature than the other *p*-type samples, BGG2 and BGG1. These observations are consistent with a gradual change toward a lower charge carrier concentration with increasing heat treatment for samples remaining *p*-type.

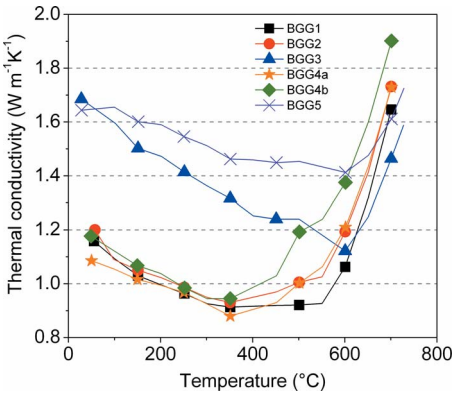

FIG. 5. (Color online) Thermal conductivity as a function of temperature for the $Ba_8Ga_{16}Ge_{30}$ samples described in Table I.

4. Thermal conductivity

The measured temperature-dependent thermal conductivity is presented in Fig. 5 for all samples studied. Two general trends can be observed for the *p*- and *n*-type samples, respectively. The *p*-type samples show very low thermal conductivity, as low as 0.9 W/m K for BGG4a and a minimum around 350 °C, where sample BGG1 has a more extended minimum up to 500 °C. The samples of *n*-type show a higher thermal conductivity and a minimum at 600 °C, due in part to the higher electronic contribution to the thermal conductivity. The minimum in κ for the *p*-type samples occurs at slightly lower temperature than the maximum in electrical resistivity, and before $|S|$ reaches its peak value. For the *n*-type samples the minimum in κ coincides with the rather weak maximum in electrical resistivity and also has a good agreement with the $|S|$ maximum. The increase in κ at high temperatures is connected with the excitation of minority carriers (bipolar thermal conduction). At the transition a rapid increase in charge carriers, of either type, will boost the electronic part of κ and, thus, increase the overall thermal conductivity.

5. Figure of merit, ZT

The *ZT*, calculated from the presented results, of all samples in the study can be seen in Fig. 6. *ZT* of the *p*-type $Ba_8Ga_{16}Ge_{30}$ is fairly stable after treatment up to 400 °C, where a small reduction in the thermopower has a negative effect on *ZT* compared to the as-prepared sample. For temperatures above 400 °C loss of gallium results in reduced extrinsic hole concentration. For BGG3 the gallium loss leads to an *n*-type material with the *ZT* peak at a lower temperature than the *n*-type reference. For the BGG4 samples the loss of gallium results in a near intrinsic material, and as a consequence of this the *ZT* value is drastically reduced and the peak temperature lowered. Overall, the reference *n*-type sample BGG5 has the highest *ZT* value, which exceeds 0.6 at 700 °C without reaching its maximum within the measured temperature range and for the *p*-type sample the as-prepared BGG1 exhibits the highest *ZT*, reaching 0.5 around 500 °C.

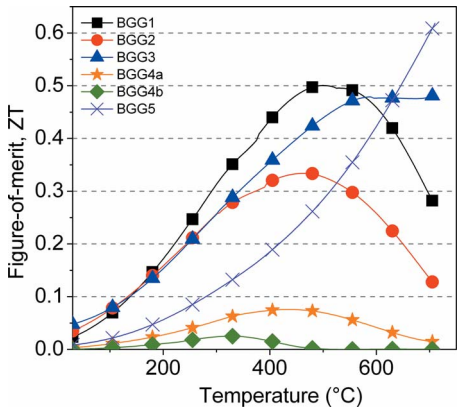

FIG. 6. (Color online) The figure of merit, *ZT*, as a function of temperature for the $Ba_8Ga_{16}Ge_{30}$ samples presented in Table I. The *p*-type samples all reach the maximum at lower temperatures than the *n*-doped samples.

IV. CONCLUSIONS

The thermal stability of *p*-type $Ba_8Ga_{16}Ge_{30}$ has been tested through a series of heat treatments of samples from a single batch of as-prepared *p*-type $Ba_8Ga_{16}Ge_{30}$. The effect of heat treatment on thermopower, electrical resistivity, and thermal conductivity has been evaluated for the thermally treated samples and compared to two as-prepared samples of *n*- and *p*-type, respectively. A significant weight reduction in the crystals, exceeding 10 wt %, due to the heat treatment was observed and ascribed to loss of gallium. Density measurements reveal that the as-prepared crystals contain voids since the density reaches the theoretical value only after grinding. However, the density is unchanged by the thermal treatment despite the loss of gallium because of the small difference in density between gallium and $Ba_8Ga_{16}Ge_{30}$. Powder XRD shows that the structure remains type-I clathrate for all heat treatments studied.

The TE evaluation reveals that the temperature at which *p*-doped $Ba_8Ga_{16}Ge_{30}$ is annealed greatly affects the transport properties of the material. Heat treatment at 400 °C does not change the TE properties of the sample significantly. However, at 600 °C and above, the extrinsic hole concentration of the sample drops considerably presumably due to the loss of gallium. At 600 °C the loss of gallium changes the majority carriers from *p*- to *n*-type, whereas the samples treated at 800 °C surprisingly remain *p*-type, but with greatly reduced hole concentration and low *ZT*. This nonuniform trend in effect of heat treatment and the underlying mechanisms for the transformation of *p*-type $Ba_8Ga_{16}Ge_{30}$ remain to be explained.

ACKNOWLEDGMENTS

The Swedish Foundation for Strategic Environmental Research (Mistra) is gratefully acknowledged for financial support through the E4 program. Swerea IVF is acknowledged for the use of the pycnometer. BSc Alex Zevalkink is thankfully acknowledged for her assistance with hot pressing of the samples at JPL. A.S. and G.J.S. thank BSc Andrew May and Dr. Eric Toberer for fruitful scientific discussions and inputs.

[1] G. A. Slack, in *CRC Handbook of Thermoelectrics*, edited by D. M. Rowe (CRC LLC, Boca Raton, FL, 1995).
[2] G. S. Nolas, J. L. Cohn, G. A. Slack, and S. B. Schujman, Appl. Phys. Lett. **73**, 178 (1998).
[3] J. L. Cohn, G. S. Nolas, V. Fessatidis, T. H. Metcalf, and G. A. Slack, Phys. Rev. Lett. **82**, 779 (1999).
[4] A. Bentien, A. E. C. Palmqvist, J. D. Bryan, S. Latturner, G. D. Stucky, L. Furenlid, and B. B. Iversen, Angew. Chem., Int. Ed. **39**, 3613 (2000).
[5] V. L. Kuznetsov, L. A. Kuznetsova, A. E. Kaliazin, and D. M. Rowe, J. Appl. Phys. **87**, 7871 (2000).
[6] N. P. Blake, S. Latturner, J. D. Bryan, G. D. Stucky, and H. Metiu, J. Chem. Phys. **115**, 8060 (2001).
[7] B. C. Chakoumakos, B. C. Sales, and D. G. Mandrus, J. Alloys Compd. **322**, 127 (2001).
[8] S. Paschen, W. Carrillo-Cabrera, A. Bentien, V. H. Tran, M. Baenitz, Y. Grin, and F. Steglich, Phys. Rev. B **64**, 214404 (2001).
[9] J. D. Bryan, N. P. Blake, H. Metiu, G. D. Stucky, B. B. Iversen, R. D. Poulsen, and A. Bentien, J. Appl. Phys. **92**, 7281 (2002).
[10] H. Anno, M. Hokazono, M. Kawamura, and K. Matsubara, in *Proceedings of the 22nd Conference on Thermoelectrics* (IEEE, New York, 2003), pp. 121–126.
[11] A. Bentien, S. Paschen, V. Pacheco, Y. Grin, and F. Steglich, in *Proceedings of the 22nd Conference on Thermoelectrics* (IEEE, New York, 2003), pp. 131–133.
[12] G. K. H. Madsen, K. Schwarz, P. Blaha, and D. J. Singh, Phys. Rev. B **68**, 125212 (2003).
[13] M. Beekman, J. Gryko, H. F. Rubin, J. A. Kaduk, W. Wong-Ng, and G. S. Nolas, in *Proceedings of the 24th International Conference on Thermoelectrics* (IEEE, New York, 2005), pp. 219–222.
[14] D. Huo, T. Sakata, T. Sasakawa, M. A. Avila, M. Tsubota, F. Iga, H. Fukuoka, S. Yamanaka, S. Aoyagi, and T. Takabatake, Phys. Rev. B **71**, 075113 (2005).
[15] H. Anno, H. Fukushima, K. Koga, K. Okita, and K. Matsubara, in *Proceedings of the 25th International Conference on Thermoelectrics* (IEEE, New York, 2006), pp. 36–39.
[16] M. A. Avila, K. Suekuni, K. Umeo, H. Fukuoka, and T. Takabatake, Phys. Rev. B **74**, 125109 (2006).
[17] N. L. Okamoto, K. Kishida, K. Tanaka, and H. Inui, J. Appl. Phys. **100**, 073504 (2006).
[18] S. Johnsen, B. Thomsen, M. Christensen, G. Madsen, M. Nygren, and B. B. Iversen, in *Proceedings of the 26th International Conference on Thermoelectrics* (IEEE, New York, 2007), pp. 219–222.
[19] J. Martin, G. S. Nolas, H. Wang, and J. Yang, J. Appl. Phys. **102**, 103719 (2007).
[20] N. L. Okamoto, K. Kishida, K. Tanaka, and H. Inui, J. Appl. Phys. **101**, 113525 (2007).
[21] M. A. Avila, K. Suekuni, K. Umeo, H. Fukuoka, S. Yamanaka, and T. Takabatake, Appl. Phys. Lett. **92**, 041901 (2008).
[22] S. K. Deng, X. F. Tang, P. Li, and Q. J. Zhang, J. Appl. Phys. **103**, 073503 (2008).
[23] N. L. Okamoto, T. Nakano, K. Tanaka, and H. Inui, J. Appl. Phys. **104**, 013529 (2008).
[24] E. S. Toberer, M. Christensen, B. B. Iversen, and G. J. Snyder, Phys. Rev. B **77**, 075203 (2008).
[25] M. Christensen, S. Johnsen, M. Sondergaard, J. Overgaard, H. Birkedal, and B. B. Iversen, Chem. Mater. **21**, 122 (2009).
[26] A. Saramat, E. S. Toberer, A. F. May, and G. J. Snyder, J. Electron. Mater. **38**, 1423 (2009).
[27] A. Saramat, G. Svensson, A. E. C. Palmqvist, C. Stiewe, E. Mueller, D. Platzek, S. G. K. Williams, D. M. Rowe, J. D. Bryan, and G. D. Stucky, J. Appl. Phys. **99**, 023708 (2006).
[28] M. Christensen and B. B. Iversen, Chem. Mater. **19**, 4896 (2007).
[29] H. Anno, M. Hokazono, M. Kawamura, J. Nagao, and K. Matsubara, in *Proceedings of the 21st International Conference on Thermoelectrics* (IEEE, New York, 2002), pp. 77–80.
[30] A. Bentien, M. Christensen, J. D. Bryan, A. Sanchez, S. Paschen, F. Steglich, G. D. Stucky, and B. B. Iversen, Phys. Rev. B **69**, 045107 (2004).
[31] M. Christensen, F. Juranyi, and B. B. Iversen, Physica B **385-386**, 505 (2006).
[32] M. Christensen, N. Lock, J. Overgaard, and B. B. Iversen, J. Am. Chem. Soc. **128**, 15657 (2006).
[33] S. K. Deng, X. F. Tang, and Q. J. Zhang, J. Appl. Phys. **102**, 043702 (2007).
[34] H. Anno, M. Hokazono, H. Takakura, and K. Matsubara, in *Proceedings*

of the 24th International Conference on Thermoelectrics (IEEE, New York, 2005), pp. 102–105.
[35]S. Johnsen, A. Bentien, G. K. H. Madsen, M. Nygren, and B. B. Iversen, Phys. Rev. B **76**, 245126 (2007).
[36]M. Christensen, G. J. Snyder, and B. B. Iversen, in *Proceedings of the 25th International Conference on Thermoelectrics* (IEEE, New York, 2006), pp. 40–43.
[37]C. Kittel, *Introduction to Solid State Physics*, 8th ed. (Wiley, Hoboken, N.J., 2005).
[38]L. R. Danielson, S. Matsuda, and V. Raag, in Proceedings of the 19th International Energy Conversion Engineering Conference, San Francisco, CA, 1984 (unpublished), pp. 2256–2259.
[39]J. Martin, H. Wang, and G. S. Nolas, Appl. Phys. Lett. **92**, 222110 (2008).
[40]I. Fujita, K. Kishimoto, M. Sato, H. Anno, and T. Koyanagi, J. Appl. Phys. **99**, 093707 (2006).
[41]E. N. Nenghabi and C. W. Myles, Phys. Rev. B **77**, 205203 (2008).
[42]A. Bentien, *Transport and Magnetic Properties of Rare-Earth Containing Clathrates and Clathrate-Like Compounds* (Shaker, Aachen, Germany, 2005).
[43]S. Johnsen, A. Bentien, G. K. H. Madsen, M. Nygren, and B. B. Iversen, in *Proceedings of the 24th International Conference on Thermoelectrics* (IEEE, New York, 2005), pp. 211–214.
[44]N. F. Mott, *Conduction in Non-Crystalline Materials*, 2nd ed. (Clarendon, Oxford, 1993).
[45]W. Carrillo-Cabrera, S. Budnyk, Y. Prots, and Y. Grin, Z. Anorg. Allg. Chem. **630**, 2267 (2004).
[46]*Chemistry, Structure, and Bonding of Zintl Phases and Ions*, edited by S. M. Kauzlarich (VCH, Copenhagen, NY, 1996).
[47]G. J. Snyder and E. S. Toberer, Nature Mater. **7**, 105 (2008).
[48]H. J. Goldsmid and J. W. Sharp, J. Electron. Mater. **28**, 869 (1999).
[49]A. F. May, E. S. Toberer, A. Saramat, and G. J. Snyder, Phys. Rev. B **80**, 125205 (2009).